EPSL-09025; No of Pages 16

Available online at www.sciencedirect.com
ScienceDirect

ELSEVIER

Earth and Planetary Science Letters xx (2007) xxx–xxx

EPSL

www.elsevier.com/locate/epsl

Temporal evolution of long-period seismicity at Etna Volcano, Italy, and its relationships with the 2004–2005 eruption

Ivan Lokmer [a,*], Gilberto Saccorotti [b], Bellina Di Lieto [c], Christopher J. Bean [a]

[a] *Seismology and Computational Rock Physics Laboratory, School of Geological Sciences, University College Dublin, Belfield, Dublin 4, Ireland*
[b] *Istituto Nazionale di Geofisica e Vulcanologia - Sezione di Pisa, Via della Faggiola, 32 - 56126 Pisa, Italy*
[c] *Dipartimento di Fisica "E. R. Caianiello", Universita degli Studi di Salerno, Via S. Allende, I-84081 Baronissi (SA), Italy*

Received 1 March 2007; received in revised form 30 October 2007; accepted 11 November 2007

Editor: C.P. Jaupart

Abstract

Between December 2004 and August 2005, more than 50,000 long-period events (LP) accompanied by very-long period pulses (VLP) were recorded at Mt. Etna, encompassing the effusive eruption which started in September 2004. The observed activity can be explained by the injection of a gas slug formed within the magmatic column into an overlying cavity filled by either magmatic or hydrothermal fluids, thus triggering cavity resonance. Although a large number of LP events exhibit similar waveforms before the eruption, they change significantly during and after the eruption. We study the temporal evolution of the LP-VLP activity in terms of the source movement, change of the waveforms, temporal evolution of the dominant resonance frequencies and the source Q factor and changes in the polarization of the signal. The LP source locations before and after the eruption, respectively, do not move significantly, while a slight movement of the VLP source is found. The intensity of the LP events increases after the eruption as well as their dominant frequency and Q factor, while the polarization of the signals changes from predominantly transversal to pure radial motion. Although in previous studies a link between the observed LP activity and the eruption was not found, these observations suggest that such a link was established at the latter end of the eruptive sequence, most likely as a consequence of a reestablishment of the pressure balance in the plumbing system, when it was undermined due to discharge of large amounts of resident magma during the eruption. Based on the polarization properties of the signal and geological setting of the area, a fluid-filled crack is proposed as the most likely source geometry. The spectral analysis based on the autoregressive-models (SOMPI) is applied to the signals in order to analyse the resonance frequencies and the source Q-factors. The results suggest water and basalt with the low gas volume fraction as the most likely fluids involved in the source process. Using theoretical relations for the "slow waves" radiated from the fluid-filled crack, we also estimate the crack size for both fluids, respectively.

Keywords: volcano seismology; long-period seismicity; Etna volcano; volcano monitoring

1. Introduction

The observation and modelling of seismic waves in volcanic settings is of great importance to enhance our

* Corresponding author. Tel.: +353 1 7162079; fax: +353 1 2837733.
E-mail address: ivan.lokmer@ucd.ie (I. Lokmer).

0012-821X/$ - see front matter © 2007 Elsevier B.V. All rights reserved.
doi:10.1016/j.epsl.2007.11.017

understanding of the physical processes in magmatic and hydrothermal systems. Long-period (LP) and very-long-period (VLP) seismicity is of particular interest because it has been widely observed in association with eruptive activity (e.g. Neuberg et al., 1994; Chouet et al., 1994, Q1 1997; Neuberg et al., 1998; Rowe et al., 1998; Matsubara and Yomogida, 2004). It is now well-established that LP events are linked to the resonance of the fluid-filled Q2 cracks and conduits (Chouet, 1996a,b, 2003; Neuberg, 2000, and references therein), while VLP activity reflects inertial forces related to the mass transport phenomena within the magmatic and hydrothermal systems (Ohminato et al., 1998; Chouet 2003). The spectral characteristics of both types of signals can be employed to probe the fluid-driven processes in volcanic environments and the state of the fluids involved in such processes.

Although Mt. Etna is the biggest volcano in Europe and one of the most active volcanoes in the world, there was only one report on the LP activity on Mt. Etna (Falsaperla et al., 2002) before the permanent broadband network installation in November 2003. The network includes 8 Nanometrics TRILIUM seismometers with flat amplitude response between 0.025 and 100 Hz, at distance between 1.5 and 9 km from the summit craters (Fig. 1). These instruments have been recording sustained LP activity for the past 3 years, thus encompassing the 'silent' effusive 2004–2005 eruption. Along with LP, weak VLP pulses were recorded, usually (but not always) preceding the onset of LP events. Saccorotti et al. (2007) presented accurate locations for both types of events and performed detailed analysis of the LP and VLP wavefield for an extended period preceding the onset of the 2004–2005 eruption (Corsaro and Miraglia, 2005; Burton et al., 2005; Di Grazia et al., 2006). Based on the absence of systematic changes of the activity throughout the analysed time interval, the authors found no obvious link between LP activity and the eruption, a result that is in agreement with the observations by Burton et al. (2005) and Di Grazia et al. (2006) who characterised the eruption as an effusion of the remnant lava stored in the superficial reservoir, triggered by the pure geodynamical forces.

During the eruption, the signature of recorded LP signals started to exhibit significant changes in terms of ~~a~~ dominant frequency and attenuation. Since this type of signals can be viewed as the oscillatory response to a fluid-filled resonator triggered by a time-localised excitation, they enable us to determine characteristic properties of the resonator by investigating the resonant frequencies and attenuation of the LP oscillations. Kumagai and Chouet (2000) interpreted these parameters and their temporal variations for various active volcanoes using the acoustic properties of a crack containing magmatic and

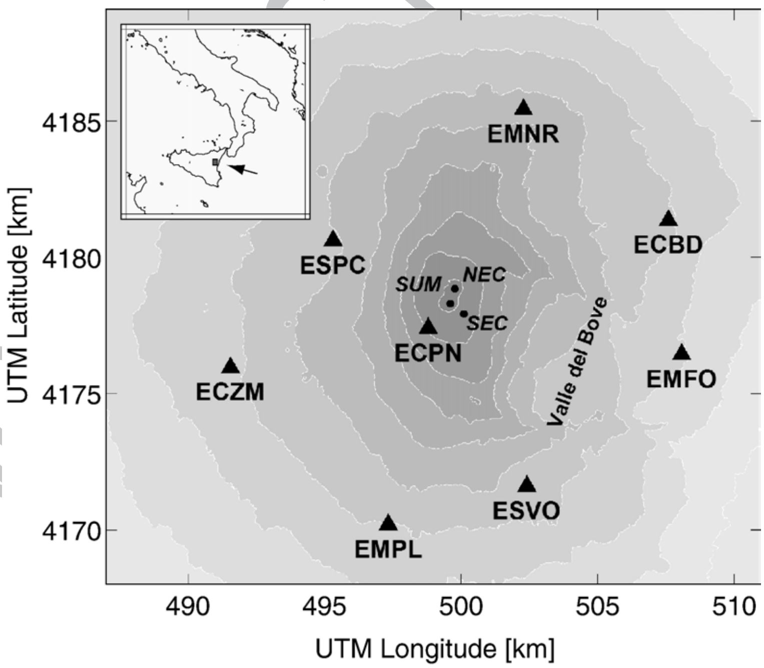

Fig. 1. Topography of Mt. Etna and broad-band seismic network. Triangles represent the seismic stations, while the solid black circles mark the positions of the main craters: SUM — Summit Craters area; NEC — North-East Crater; SEC — South-East Crater. The interval between the contours is 300 m, starting from an elevation of 3200 m a.s.l. (the elevation of the summit of Etna is 3320 m a.s.l.). The inset shows the location of Etna with respect to Italy.

Please cite this article as: Lokmer, I., et al., Temporal evolution of long-period seismicity at Etna Volcano, Italy, and its relationships with the 2004–2005 eruption, Earth Planet. Sci. Lett. (2007), doi:10.1016/j.epsl.2007.11.017

hydrothermal fluids. In this paper, we extend the observations of Saccorotti et al. (2007) to the period after the eruption and study the temporal evolution of LP-VLP activity, in terms of the source movement, change of the signal signature, temporal evolution of the dominant resonant frequencies and the source Q factors and changes in the polarisation of the signal. The observed temporal evolution of the signal can be directly mapped to the temporal evolution of the LP source. Our aim is to establish a dynamical framework for the observed LP activity and find a possible one-way coupling between the eruption and LP activity. We also estimate the size of the LP source.

2. LP-VLP activity 2004–2005

2.1. Data

Sustained LP activity has been recorded since a permanent broadband network was installed at Mt. Etna in November 2003 (Fig. 1). LP events were detected by an automatic routine based on the spectral correlation between time-windows of the continuous record and a characteristic LP spectrum obtained by averaging spectra from a set of visually-selected events. For each event, the RMS value of the displacement magnitude (all 3 components) was calculated for the ECPN station (Fig. 2a). Saccorotti et al. (2007) demonstrated a high level of waveform similarity between events recorded before the eruption. Events recorded a few months after the eruption are also found to be similar to each other. This made it possible to analyse only the most energetic signals, denoted by the dark-grey dots in the Fig. 2a, as representative of the complete dataset. Before the analysis the instrument response was removed and the recorded velocity was transformed to displacement. An example of such processed seismograms recorded at the ECPN station a few months before and a few months after the eruption, is shown in Fig. 2b. In both cases, the LP signal is preceded by the VLP pulse which has a peak frequency between 0.03 and 0.05 Hz. However, in some cases VLP signal occurs alone, either like VLP tremor or a single VLP pulse not followed by LP event. Such separate occurrence of these two types of signals suggests that they belong to either different systems (Saccorotti et al., 2007) or systems which are not completely coupled. In the inset boxes of Fig. 2b, 25 seconds long band-passed waveforms (f=0.3 – 1.5 Hz) are shown. LP signals from two different periods look quite different: before the eruption the fundamental mode of oscillation is peaked at about

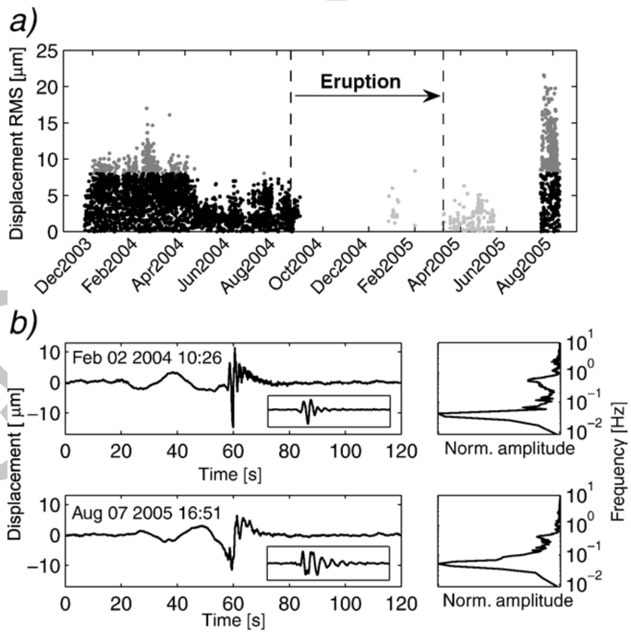

Fig. 2. RMS amplitudes and recorded waveforms. (a) RMS values of displacement recorded at ECPN station. RMS values of the signal magnitude (all 3 components) are calculated for the 6 s long time window encompassing the maximum displacement. Dark grey dots denote signals above the threshold RMS = 8 μm, which were analysed in this study. Seismograms recorded during the late eruptive stage and immediately after the eruption are denoted by light grey dots. This subset was analysed in order to have a better insight into the temporal evolution of the signal from pre-eruptive through to the post-eruptive stages. (b) Seismograms and their spectra recorded before (top) and after (bottom) the eruption. Band-pass filtered (f=0.3 – 1.5 Hz), 25 s long waveforms are shown in the inset box. Note that most energy is contained at frequencies below 1 Hz.

Please cite this article as: Lokmer, I., et al., Temporal evolution of long-period seismicity at Etna Volcano, Italy, and its relationships with the 2004–2005 eruption, Earth Planet. Sci. Lett. (2007), doi:10.1016/j.epsl.2007.11.017

0.6 Hz, while after the eruption it depicts a frequency of about 0.4 Hz and a narrower spectral peak.

The recorded sequence encompasses the effusive eruption, which occurred in the period September 2004–March 2005, thus enabling us to examine the possibility of a connection between the eruption and LP activity. However, the signals recorded during the eruption are masked by tremor during the effusive activity, so we restricted the quantitative part of our study to the LP activity before and a few months after the eruption. A subset of 225 events recorded in the period January–May 2005, during and immediately after the eruption (denoted by the light-grey dots in the Fig. 2a), was used only to obtain a qualitative picture of the temporal evolution of the signals.

2.2. Locating the events

In order to distinguish between source movement and the activity regime as the possible causes of the temporal change of the signals, we are interested in relative locations of the two subsets of events, belonging to pre- and post-eruptive periods, respectively (referred as *Period I* and *Period II*, hereinafter). Saccorotti et al. (2007) found absolute locations of the most energetic events from *Period I*, which they showed to be representative of the complete pre-eruptive sequence. They used a non-linear, probabilistic inversion (Tarantola and Vallette, 1982) acting on reciprocal travel-times calculated using finite-difference ray tracing for the 3D heterogeneous P-wave velocity structure of Patanè et al. (2002). Since we are interested only in relative locations between the two periods, we relocate events from *Period I* and locate those from *Period II*, using a simple method which minimizes a misfit function given by the L1-norm of travel time residuals for a homogeneous velocity model. The best estimate for the P-wave velocity, 2.7 km/s, is obtained as one which minimizes the misfit function obtained for all the signals and all the stations.

In order to define the confidence interval for our locations, we repeated the location procedure, adding random noise to simulate incorrect time readings and waveform arrival-time misalignments. The picking errors were assumed to be normally distributed with zero mean and 0.1 s standard deviation, while the error due to the waveforms misalignment is taken from the uniformly distributed interval −0.005–0.005 s (time sampling rate). In this way, for each event the synthetic catalog of 400 travel times was created. We then divided the whole Etna area to a grid with a cell size of 60 × 60 × 60 m, and divided the number of locations within each cell by the total number of synthetic travel times.

At the summit station (ECPN) VLP pulses acting contemporaneously with the LP activity were observed. These pulses are characterised by the rectilinear motion with an angle of incidence between 55 and 65 degrees. The free-surface correction angles were obtained from numerical simulations, using the volcano topography and a homogeneous velocity model, employing the numerical scheme described in O'Brien and Bean (2004). For a range of source depths between 500 and 2000 m, these corrections are found to be less than 2°. The absence of the VLP recordings at other stations prevented us from locating this type of activity in a conventional way. Instead, we corrected the observed incidence angles and projected the VLP polarisation vectors onto the plane passing in the E–W direction through the centre of the LP cluster. Only the data for which rectilinearity of the polarisation ellipsoid is greater than 0.9 were used. Results for both LP locations and VLP projections are given in Fig. 3.

It can be seen from the Fig. 3a that the majority of the LP hypocenters are clustered in a small volume at elevations of 1700–2900 m, i.e. depths between 400 m and 1600 m below the summit craters, which have an elevation of about 3300 m. The white dots represent the locations of events without added noise. A slight movement of the centre of the post-eruptive cluster towards the west can be observed, but it is negligible once the confidence interval is taken into consideration. Thus, the temporal changes of the LP waveforms can be attributed to different regimes of activity rather than to source movement.

Although we cannot determine the exact position of VLP source nor its spatial extent from only 1 station, the contemporaneous activity of VLP and LP sources suggests a common epicentral region for both types of activity. Assuming a vertical or inclined conduit, Fig. 3b shows a slight downward movement of the VLP source between the pre- and post-eruptive stages.

3. Data analysis

3.1. Temporal evolution of similar events

Although individual unfiltered signals exhibit different signatures, one can observe a common shape for the waveforms when they are band-pass filtered within the frequency band 0.3 – 1.5 Hz. Since this is also the most energetic part of signal, it makes it possible to infer the main characteristics of the changing source-regime through the observation of temporal changes of the signal. In order to get a qualitative idea of such changes, we performed cross-correlation between all pairs of

Please cite this article as: Lokmer, I., et al., Temporal evolution of long-period seismicity at Etna Volcano, Italy, and its relationships with the 2004–2005 eruption, Earth Planet. Sci. Lett. (2007), doi:10.1016/j.epsl.2007.11.017

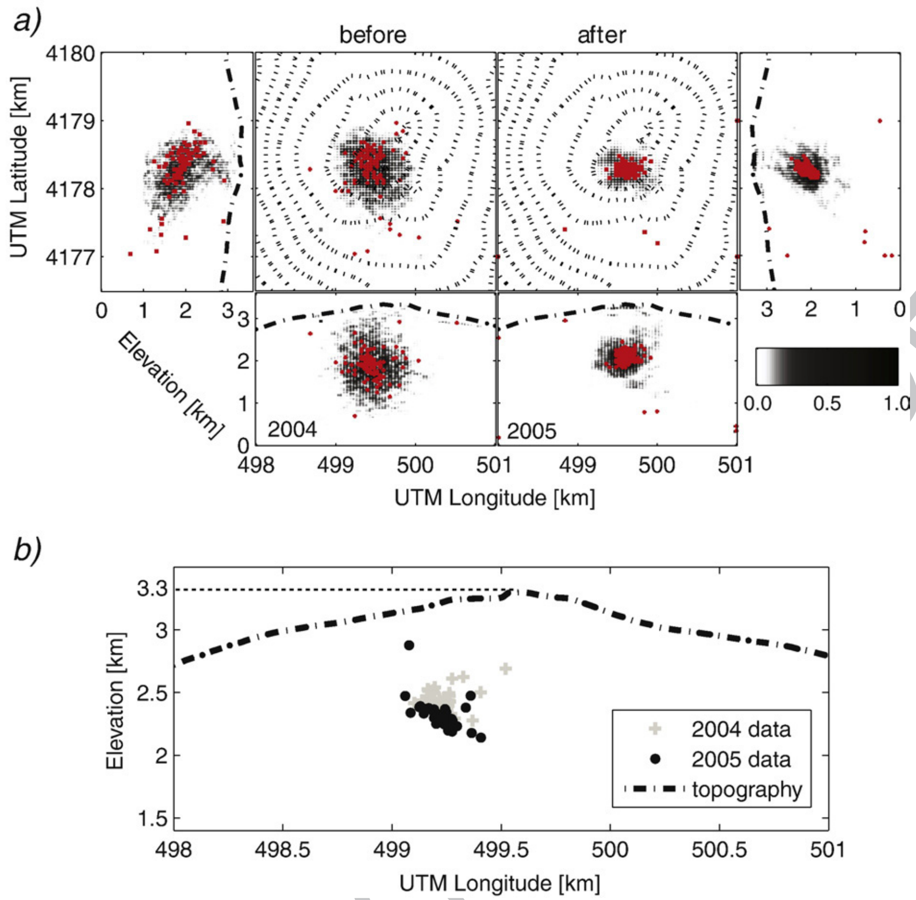

Fig. 3. LP and VLP locations. (a) Locations of the two clusters of LP events (left) before and (right) after the 2004–2005 eruption. The elevation of the summit crater is 3300 m. The red dots (white in the printed version) denote the locations of recorded events. Events are located by using a homogeneous velocity model. The confidence intervals (the shaded area) are calculated from the synthetic catalog of events obtained by adding noise to the arrival times due to the both incorrect reading of the P-wave onset and the finite time sampling. (b) Projection of the VLP polarisation vector onto the E–W vertical plane which passes through the centre of LP clusters. Data recorded before the eruption are represented by the grey crosses, the black circles denote VLP events after the eruption. Only the data for which the rectilinearity of the polarisation ellipsoid is greater than 0.9 are shown.

signals, thus defining clusters of similar events. Then, we used the inter-event time delays measured via correlation analysis to align individual signals, eventually obtaining stacked seismograms representative of each cluster. Saccorotti et al. (2007) demonstrated the similarity of signals within this frequency band for the pre-eruptive period. Their result allows us to use the most energetic event from the *Period I* as representative of the complete pre-eruptive sequence of the LP activity. The same argument holds for *Period II*. In addition to the most energetic events from *Period I* and *II*, we also used a subset of 225 events recorded in the period January–May 2005 (see Fig. 2a). 15 s long signals, encompassing their most energetic part, were cross-correlated. A cluster of similar events was defined as a set of events whose correlation coefficient was higher than 0.85 for all possible event pairs. As we have shown that there is no significant LP source movement between pre- and post-eruptive stages, this allows us to attribute temporal change of the signal to the different source regimes rather than to the source movement. The stacked signals for the 6 clusters comprising more than 30 events each, along with the temporal distribution of events belonging to each cluster, are shown in Fig. 4. An example of similar events for the cluster 1 before their stack is shown in the Fig. 4a. Although the conservative criterion applied in the cross-correlation analysis resulted in the 6 clusters, the stacked signals reveal the two main regimes of the LP activity, the first one associated with the clusters 1 and 2, and the second with the clusters 3 to 6. Regime 2 is characterised by a lower frequency and longer-lasting signal than regime 1. While the events recorded a few months before and a few months after the eruption, respectively, belong to the different regimes of LP activity, the period during

Please cite this article as: Lokmer, I., et al., Temporal evolution of long-period seismicity at Etna Volcano, Italy, and its relationships with the 2004–2005 eruption, Earth Planet. Sci. Lett. (2007), doi:10.1016/j.epsl.2007.11.017

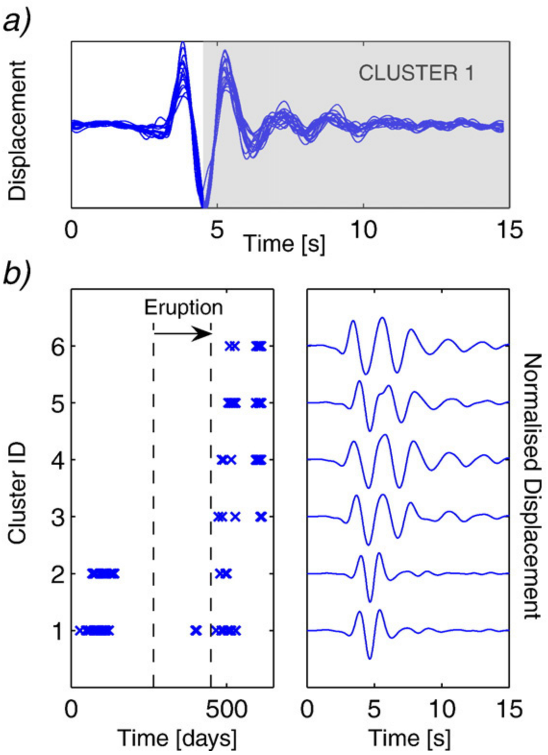

Fig. 4. Temporal evolution of the recorded signal. (a) An example of similar signals (cluster 1) where the correlation coefficient between each pair of events is higher than 0.85. The shaded part of the signal, following the maximum absolute amplitude, was used when performing the polarisation analysis (see the next paragraph). (b) Distribution of similar events over the 6 clusters and their stacked waveforms. Note that events recorded a few months before and a few months after the eruption represent two different regimes of LP activity, while events recorded during and immediately after the eruption can be seen as a transition zone between these two regimes.

and immediately after the eruption can be recognised as the transition zone between the two types of activity.

3.2. Complex frequency of different source regimes

It is known from simplified models of seismo-volcanic sources (e.g. Chouet, 1986, 1988, 1992) that the resonance frequency and damping of the system is strongly influenced by the nature of liquid and gas content. Thus, information on the change of physical properties of the fluid-driven source can be inferred by observing the temporal change of the spectral properties of signal. Kumagai et al. (2002) and Kumagai (2006) followed the temporal evolution of fluid-driven sources by the temporal change of the complex frequencies inferred from individual signals spanning a time window of a few months. Here, instead, we analyse the temporal change of the source regimes, each of which is represented by a stack of similar signals described above. Although such an approach cannot reveal subtle changes of the source within a short time window, we believe that it ensures a robust analysis of the main source properties. Ideally, we would like to recover the temporal evolution of the source resonance (change of the source frequency and Q factor) from the recorded signals. However, topography and soft superficial layers can have a detrimental effect on signal quality. Ripperger et al. (2003), using numerical simulations for the case of a homogeneous model and shallow source, demonstrated a strong

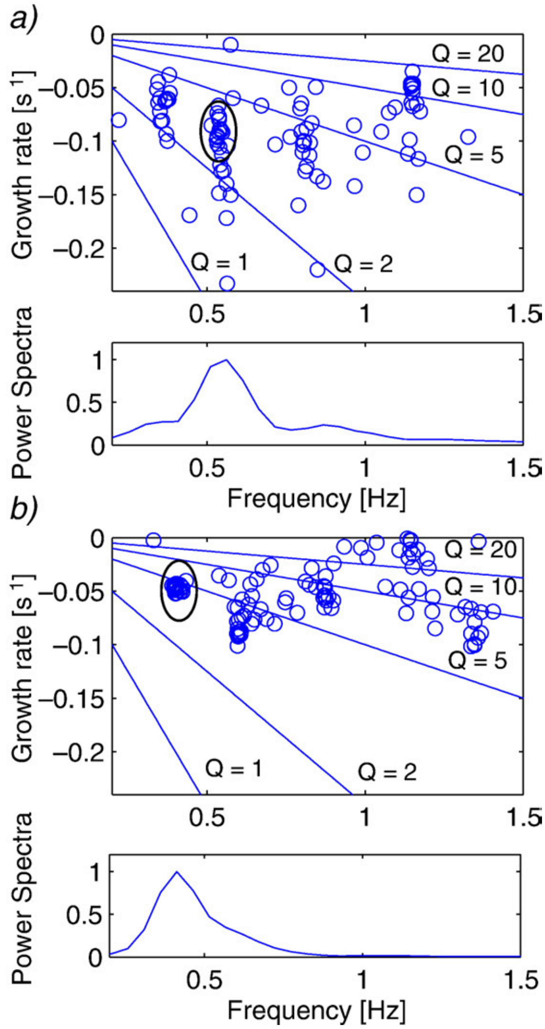

Fig. 5. Complex frequencies obtained from the SOMPI analysis. (a) (top) Complex frequencies of individual wave elements for AR orders 4–70, estimated for the stacked vertical displacement waveform associated with the cluster 1 in Fig. 9. (bottom) Amplitude spectrum of the same waveform. (b) (top) Complex frequencies estimated for the waveform associated with the cluster 6 in Fig. 9. (bottom) Amplitude spectrum of the same waveform.

influence of the volcano topography on the signal duration at the stations situated on the flanks of the Merapi volcano. Only stations very close to the summit reflect the behaviour of the source, while the others are strongly "contaminated" by the topographical surface waves. Using the numerical scheme of O'Brien and Bean (2004), we found that even stronger modification of the waveforms is expected once energy is transmitted through a shallow, soft layer, especially for the stations located on the flanks of a volcano.

In such a case, the source Q factor cannot be recovered. To minimise this effect, we restrict our analysis to the ECPN station only, which is situated near the summit crater, closest to the source.

In order to determine the complex frequencies of LP events, the SOMPI method was used (Kumazawa et al., 1990, and references therein). This is a spectral analysis method based on an autoregressive (AR) model, which addresses the problem of resolving the decaying harmonic components of a time series corrupted by noise. Due to its better resolution compared to Fourier-based spectral estimates and ability to determine damping factors as characteristic properties of a linear dynamical system, it is a powerful tool for studies dealing with resonating sources. The force-free tail of the oscillating signal is resolved into a number of harmonic components, each of them described by a complex frequency $f-ig$, where f is frequency, g is the growth rate, and i the imaginary unity. A quality factor Q is defined as $-f/2g$.

The results of SOMPI analysis of the stacked waveforms associated with the clusters 1 and 6 in Fig. 4 are shown in Fig. 5, along with their corresponding Fourier spectra. (f–g) diagrams of the complex frequency represent wave elements for AR orders 4 to 70. Densely populated regions indicate stably resolved harmonic components, while scattered points represent incoherent noise. It can be seen that LP waveforms are characterised by a drop in dominant frequency between the two regimes and a slight increase in Q. Although four oscillation modes are apparent in f–g diagrams, we analyse the lowest two peaks present in both diagrams, one of which is dominant for each regime (denoted by ellipses). The complex frequency for each waveform along with the corresponding variance is determined from AR order indicated by Akaike's information criterion (AIC) (Akaike, 1974). We use all 6 stacked waveforms, shown in Fig. 4, and determine the complex frequencies of the two modes from each of them. Finally, these frequencies are used to obtain the mean frequency and Q factor of each mode, respectively, for 2 regimes. We use the formula:

$$x_{rj} = \frac{\sum w_i(x)\cdot x_i}{\sum w_i(x)}, \quad x = f, Q, \qquad rj = \begin{cases} r1, & i = 1,2 \quad \text{(regime 1)} \\ r2, & i = 3,4,5,6 \quad \text{(regime 2)} \end{cases}, \tag{1}$$

where index rj denotes different regimes, while index i is the identification number of clusters 1 to 6. Weights, $w_i(x)$, are defined to be proportional to a number of individual waveforms belonging to a certain cluster, n_i, and inversely

Table 1
Frequencies and Q factors of the stacked waveforms and their weighted means estimated for the two regimes of the LP activity (see text for details)

Regime 1 (Combining clusters 1 and 2)	Regime 2 (Combining clusters 3 to 6)
Mode 1 (secondary mode):	*Mode 1 (dominant mode):*
f_1=0.380±0.020 Hz, Q_1=2.6±0.2, n=76	f_3=0.403±0.001 Hz, Q_3=4.72±0.1, n=27
f_2=0.375±0.006 Hz, Q_2=2.2±0.3, n=41	f_4=0.399±0.001 Hz, Q_4=4.68±0.1, n=63
	f_5=0.401±0.002 Hz, Q_5=4.55±0.1, n=47
	f_6=0.398±0.001 Hz, Q_6=4.39±0.1, n=36
Mode 2 (dominant mode):	*Mode 2 (secondary mode):*
f_1=0.540±0.010 Hz, Q_1=3.1±0.2, n=76	f_3=0.597±0.012 Hz, Q_3=5.23±0.6, n=27
f_2=0.568±0.004 Hz, Q_2=3.0±0.1, n=41	f_4=0.599±0.009 Hz, Q_4=3.9±0.2, n=63
	f_5=0.604±0.010 Hz, Q_5=4.2±0.7, n=47
	f_6=0.595±0.006 Hz, Q_6=3.6±0.2, n=36
Mode 1:	*Mode 1:*
f_{r1}=0.377±0.002 Hz, Q_{r1}=2.5±0.2	f_{r2}=0.400±0.001 Hz, Q_{r2}=4.6±0.1
Mode 2:	Mode 2:
f_{r1}=0.556±0.014 Hz, Q_{r1}=3.1±0.1	f_{r2}=0.599±0.002 Hz, Q_{r2}=4.0±0.3

Both parameters are estimated for all the clusters in Fig. 4, for the first two modes. Note that values of frequency and Q factor increase for both modes between the regime 1 and 2.

Please cite this article as: Lokmer, I., et al., Temporal evolution of long-period seismicity at Etna Volcano, Italy, and its relationships with the 2004–2005 eruption, Earth Planet. Sci. Lett. (2007), doi:10.1016/j.epsl.2007.11.017

proportional to the dispersion of frequency and Q factor estimated by the SOMPI analysis:

$$w_i(x) = n_i \cdot \frac{x_i}{\sigma_i(x)}, \quad x = f, Q, \tag{2}$$

where $\sigma_i(x)$ denotes standard deviations of f and Q, estimated by the error propagation from the time series to the characteristic frequencies (Kumazawa et al., 1990). The standard deviation of the weighted means obtained by Eq. (1) was calculated using the equation given in De Vries (1986):

$$\sigma_{rj}^2(x) = \frac{\sum w_i(x) \cdot (x_i - x_{rj})^2}{(N-1)\sum w_i(x)}, \quad x = f, Q,$$
$$rj = \begin{cases} r1, & i = 1,\ 2 \quad \text{(regime 1)} \\ r2, & i = 3,\ 4,\ 5,\ 6 \quad \text{(regime 2)} \end{cases}, \tag{3}$$

where N is a number of data used for the calculation of weighted means and standard deviations, and is equal to 2 and 4 for the regimes 1 and 2, respectively. Frequencies, Q-factors and their standard deviations for all 6 clusters obtained by the SOMPI analysis, along with the weighted means and standard deviations for the two different regimes of LP activity calculated using Eqs. (1)–(3), are given in Table 1. As seen from the table, for each individual mode, frequencies for all the clusters within a certain regime exhibit very small fluctuations and their standard deviations are also small. Somewhat bigger, but still small variations of Q factors can be observed. Bigger variations in Q factors with respect to frequency are usually observed because Q factors are more sensitive to the level of noise as well as to the adopted order of the AR model. However, here we used stacked waveforms with low noise levels and only the data recorded at the station which is closest to the source. Therefore, we are confident that estimated frequencies and Q factors reflect reasonably well the behaviour of the LP source. The most noticeable feature of the temporal evolution of the oscillating source is a switching of the dominant and secondary mode between two regimes, accompanied with a slight increase in frequency and Q factor for both of them, respectively. The same trend in frequency and Q factor can be observed for the two secondary modes of oscillation present in Fig. 5, but due to their very low energy and possible higher contamination by noise, they were not included in the quantitative analysis.

3.3. Polarisation analysis

Chouet (1986) investigated far-field radiation patterns of P and S waves radiated from an oscillating fluid-filled crack. In Chouet (1988), he expands his study showing a few profiles of seismograms recorded in the near- and intermediate-field, where standing waves patterns of the oscillating crack surface are clearly observed. He suggests that such an observation should provide a powerful tool to define the extent of the source by analysing the relative content of energy belonging to different modes of resonance, provided that the observation is made using a small-aperture array. However, our observations show that for either of two regimes the source oscillates with predominantly one frequency. In such a monochromatic case, even one near-to-intermediate-field station could enable us to gain an idea about the nature of the resonance. Therefore, we performed polarisation analysis of recorded signals, using the covariance-matrix method of Kanasewich (1981). We calculated all 3 axes of the polarisation ellipsoid for a 5 seconds window for each signal, starting from its maximum absolute amplitude (shaded region in the Fig. 4a). We plotted projections of the obtained axes onto horizontal, radial-vertical and transverse-vertical planes passing through the receiver

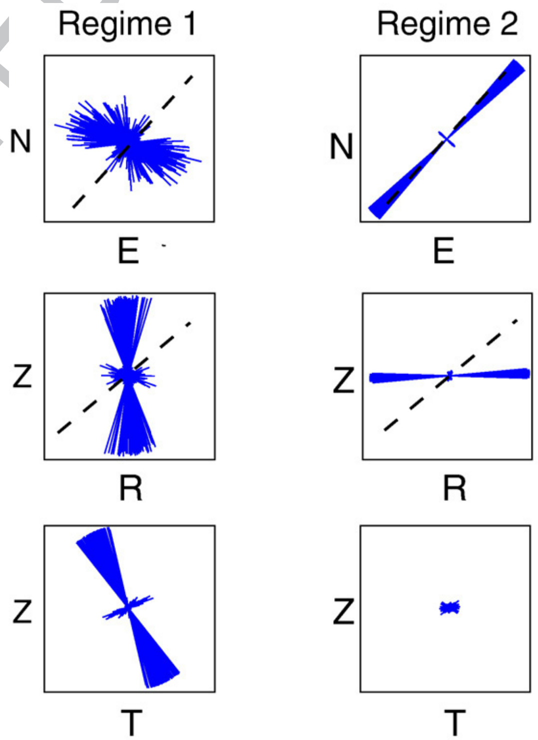

Fig. 6. Main axis of polarisation ellipsoid of the signal projected to the (top) horizontal, (middle) radial–vertical and (bottom) transversal–vertical plane. Polarisation of the signals belonging to the regime 1 and 2 is shown on the left and right panels, respectively. Note the absence of the major radial motion before the eruption, while after the eruption the particle motion is predominantly radial.

Please cite this article as: Lokmer, I., et al., Temporal evolution of long-period seismicity at Etna Volcano, Italy, and its relationships with the 2004–2005 eruption, Earth Planet. Sci. Lett. (2007), doi:10.1016/j.epsl.2007.11.017

position, for both regimes, respectively. Results are shown in Fig. 6. The dashed line in the figure denotes source–receiver direction. While particle motion before the eruption was characterised by predominantly transverse and vertical motion, after the eruption it turns into horizontal–radial motion. For the case of a single source, this observation eliminates a spherical cavity as a possible source candidate and implies a non-isotropic source, in agreement with Saccorotti et al. (2007). The main question arising here is if it is possible that longitudinal and transverse modes of the crack resonance excite different radiation patterns. Detailed discussion on this matter follows in the next section.

4. Discussion

Saccorotti et al. (2007) analysed a sequence of LP activity occurring from November 2003 to the onset of the effusive eruption on September 7th 2004. Observed non-destructive repetitive LP activity accompanied by VLP pulses was explained as a resonance of a cavity filled by magmatic or hydrothermal fluids at a poor gas volume fraction, triggered by injection of gas exolved from the nearby magmatic column. The same authors suggest that there is no connection between the LP activity and the eruption. Due to the absence of typical seismological precursors (Di Grazia et al., 2006), and geochemical properties of extruded lavas (Burton et al., 2005), the eruption was characterised as an effusion of the remnant lava stored in the superficial reservoir, triggered by geodynamical forces associated with steep topography on the eastern flank of the volcano. However, our current observations of temporal changes of the seismological parameters during and after the eruption seem to suggest the possibility of one-way coupling between the eruption and LP activity. These observations can be summarised as follows:

- No movement of the LP source within confidence intervals
- Slight movement of the VLP source
- Increase in intensity of LP events
- Increase in resonance frequency and source Q-factor
- Change in the polarisation of the signal

In the next section, we propose a model for the link between the eruption and the change of the LP regime, which explains the observations outlined above. Then we discuss the link between the longitudinal/transverse mode of a vibrating crack and the polarisation of the observed signal. Finally, we estimate the size of the source.

4.1. Link between eruption and LP regime

Both this study and that of Saccorotti et al. (2007) determine a shallow source at elevations mainly between 1700 m and 2900 m, i.e. depths between 400 and 1600 m below the summit crater (3300 m a.s.l.). Based on seismic wave attenuation and velocity tomography, two groups of authors (De Gori et al., 2005; Martínez-Arévalo et al., 2005) suggest that the upper part of this region consists of fractured, fluid-filled hot rock surrounding the molten material. Although little attention has been given to the presence of water in the upper parts of Etna volcano, a few recent studies, using dipole geoelectric, magnetotelluric and self-potential methods (e.g., Mauriello et al., 2004; Della Monica et al., 2004; Manzella and Zaja, 2006) as well as phreatomagmatic activity at the Piano del Lago site at 2570 m a.s.l. during the 2001 eruption reported by Behncke and Neri (2003), suggest the existence of groundwater within the first 500 m below ground level. The deformation study conducted by Bonaccorso and Davis (2004) describes two classes of final magma penetration at Mt. Etna: dykes that propagate horizontally and vertically. Following these authors, the first class of dykes propagate from the summit craters to the eruption point, thus supplying magma to the flanks from the deeper magma reservoir through the summit conduit zone. Their extension is mostly in a NW–SE direction at a typical depth of 500–1000 m. In summary, we can suggest that the LP activity originates in the region with the following characteristics:

1) possible interaction between magmatic and fractured hydrothermal system,
2) bending point of the magma transport from depth towards the flanks, and
3) presence of the fractured region towards the SE flanks where the 2004 eruption occurred.

Features 1) and 2) support the LP model suggested by Saccorotti et al. (2007), outlined in Section 1. Moreover, the different time delays and amplitude correlation between VLP and LP signals observed by the same authors suggest that they are inter-related but represent different mechanisms, which supports the interpretation of the interaction between two systems. The presence of the proposed fracture zone at Mt. Etna between the source position and the eruption site opens a possibility of depressurisation of the source region due to the void left by the erupted magma. According to Sturton and Neuberg (2003), decompression of magma can move the bubble nucleation level deeper in the system by a few hundred

Please cite this article as: Lokmer, I., et al., Temporal evolution of long-period seismicity at Etna Volcano, Italy, and its relationships with the 2004–2005 eruption, Earth Planet. Sci. Lett. (2007), doi:10.1016/j.epsl.2007.11.017

metres. This will increase the size of the gas slug arriving at the terminal part of the magmatic column. In such a case, the apparent VLP source location will move downwards, as observed here (Fig. 3b). Since the gas slug reaching the terminal part of the magmatic column is more energetic than in the period before the eruption, an increase in size of LP events is expected, as observed (Fig. 2a).

In a state of equilibrium, the pressure within a fluid-filled crack is equal to the ambient pressure of the source region. When gas is injected, this pressure exceeds the ambient pressure and the excess of a gas–fluid mixture is discharged into surrounding area, which triggers the LP oscillations. This discharge explains the observed dilatation at the onset of recorded signals (Fig. 4). Fluid discharges through the crack edge determined by the local stress conditions. Thus, a change in these conditions can change the direction in which the crack is discharged, which leads to the change of the principal mode of the crack resonance. However a detailed analysis of the geodynamical stress field is out of the scope of this study.

Another observation which also supports the proposed model is the increase in frequency and source Q-factor for the both modes of the source resonator, respectively (see Fig. 5 and Table 1). Using Henry's law for the liquid–gas solution, Kumagai (2006) showed that gas volume fraction in the gas–liquid mixture increases with decreasing pressure. The same author, using the crack model of Chouet (1986), showed that for basalt-gas mixture a very slight increase in frequency and a larger increase in Q-factor is expected for an increased volume fraction of gas in the mixture (Fig. 6 in Kumagai, 2006). Similar behaviour is expected for the bubbly water, but with a higher increase in frequency, as shown by Kumagai et al. (2002) in Fig. 7.

4.2. Mode of oscillation and particle motion

Crack opening/closing can be described by a system of equivalent forces for which, in the case of a vertical crack oriented as in Fig. 7a, the moment tensor has a form (Aki and Richards [47], equation 3.21):

$$M \propto \pm \begin{bmatrix} \lambda + 2\mu & 0 & 0 \\ 0 & \lambda & 0 \\ 0 & 0 & \lambda \end{bmatrix}, \tag{4}$$

where λ and μ are Lamé's constants, and signs "+" and "−" denote crack opening and closing, respectively. The set of equations (4.29) from Aki and Richards (2002), re-

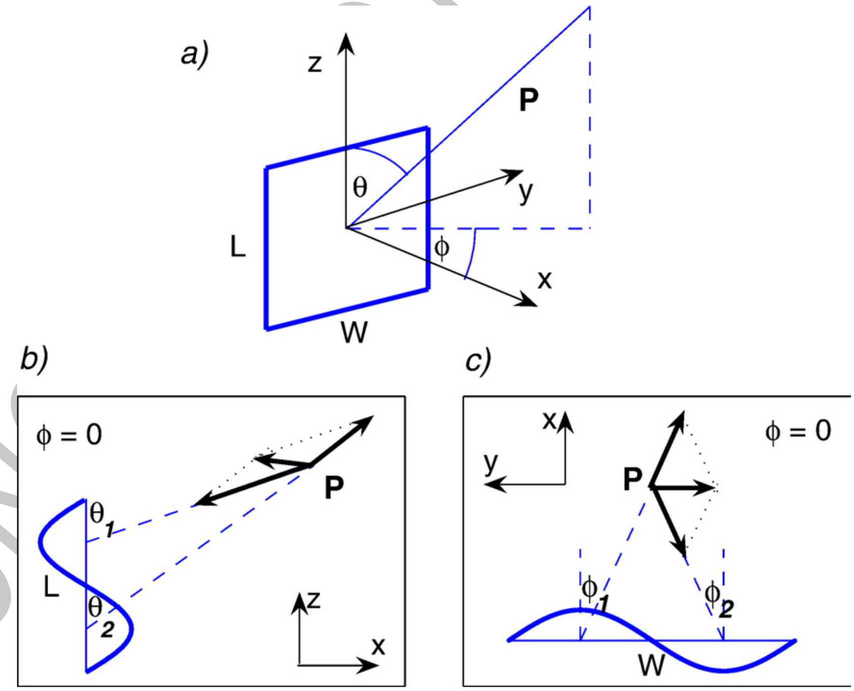

Fig. 7. Schematic of the P-wave radiation from the longitudinal and transversal crack resonance, respectively. (a) Spherical coordinate system with the origin in the centre of the vertical crack. (b) Longitudinal mode of resonance for a source–receiver azimuth $\phi = 0°$. Note that particle motion always remains polarised in the P–SV plane. (c) Transversal mode of resonance viewed from above. Motion in the transversal direction is created. For simplicity, only one crack wall is shown in the figure.

Please cite this article as: Lokmer, I., et al., Temporal evolution of long-period seismicity at Etna Volcano, Italy, and its relationships with the 2004–2005 eruption, Earth Planet. Sci. Lett. (2007), doi:10.1016/j.epsl.2007.11.017

written in the spherical coordinate system (see Fig. 7a) and by taking $\lambda = \mu$, gives a displacement field due to a moment-tensor defined by Eq. (4) as follows:

$$
\begin{aligned}
u^r &= (P^F - P^I + 2S^I - 6N) + 2\sin^2\theta\cos^2\phi \\
&\quad \times (P^F + 4P^I + 3S^I + 9N) \\
u^\theta &= \sin 2\theta\cos^2\phi \cdot (2P^I + 3S^I + S^F - 6N) \\
u^\phi &= -\sin\theta\sin 2\phi \cdot (-2P^I + 3S^I + S^F - 6N)
\end{aligned}
\tag{5}
$$

where P^F, S^F, P^I, S^I and N are functions of travel-time, source–receiver distance, properties of the medium, seismic-moment and the source time-history. P^F and S^F denote far-field P- and S-waves, P^I and S^I intermediate-field P and S terms and N stands for the near-field term. Note that the dependence of u^r, u^θ and u^ϕ on direction of propagation is common for the far-, intermediate- and near-field disturbance propagating through the medium. This property of the source mechanism described by Eq. (4) makes the following discussion more general.

For the fluid-filled crack, at the time $t = 0$, when resonance is triggered, the initial pulse propagates through the medium at P- and S-wave velocities and a displacement field given by Eq. (5) is recorded at the receiver. At the same time slow interface waves start to propagate along the crack walls with a velocity slower than the acoustic velocity of fluid (Chouet, 1986; Ferrazzini and Aki, 1987), thus sustaining the oscillation of the crack. According to Ferrazzini and Aki (1987), these waves cannot be directly observed at distances greater than a wavelength, which for the case of the fundamental mode of resonance, is equal to the crack length. However, due to the finite dimensions of the crack, the strong horizontal motion in the fluid layer can provide an important source of radiation which can be observed at large distances. Chouet (1988) showed that this type of disturbance can be recorded at near and intermediate distances. For the fundamental mode of the crack resonance, $\lambda = L$, where λ is the wavelength of the fundamental mode and L is the crack length, and the source-receiver azimuth $\phi = 0$, a schematic of the P-wave propagation for the longitudinal and transversal mode of the crack oscillation is given in the Fig. 7b and c, respectively. Similar considerations can be undertaken for SV and SH waves. Note that although Eqs. (5) give $u^\phi = 0$ for a vertical crack observed at an azimuth $\phi = 0$, transverse motion is generated. Such an oscillating crack can be described by two simultaneously acting, closely spaced sources whose mechanisms are given by Eq. (4), but have opposite signs. In the case considered in this study, the seismic station is in close proximity to the source (see Fig. 1). Following this simple deduction we suggest that different polarisations in the wave train before and after the eruption can be explained by the excitation of perpendicular modes of source resonance. This interpretation is qualitative, and a full moment-tensor inversion needs to be performed to obtain the source mechanism and its orientation. This is a subject of further work.

An important implication of the observation outlined above is that the moment-tensor solution could be sensitive to the direction of the slow waves propagating along the crack walls. However, future work is required to confirm this hypothesis.

4.3. Slow waves and source size

Quasi-monochromatic long-period seismograms, such as observed on Etna, can be successfully explained by the existence of slow waves propagating along the fluid–solid interface between the fluid-filled resonator and surrounding medium, with a velocity lower than the acoustic velocity of fluid. These waves were first detected in the models of Chouet and Julian (1985) and Chouet (1986), who found that the resonance period of the fluid-filled crack can be much longer than that expected from the acoustic properties of fluid and size of the resonator. Chouet (1986) called them "crack waves". He also found that the phase velocity of the crack wave rapidly decreases with increasing values of a non-dimensional parameter called the crack stiffness, C, originally introduced by Aki et al. (1977):

$$
C = \frac{b}{\mu}\frac{L}{h} \tag{6}
$$

where b is the bulk modulus of the fluid, μ is rigidity, L is the length of the crack and h its aperture. Since the crack wave velocity depends on the crack stiffness, it is a crucial parameter for estimating the size of a fluid-filled resonator. Following the work of various authors, Chouet (1988) gives estimates for possible in-situ values of the crack stiffness. Thus, for dykes filled with basalt this parameter is estimated to be between 10 and 500, while for hydrofractures values range from 10^3 to 10^4. Saccorotti et al. (2007) showed that the low values of the source Q factor estimated from our signals support both types of fluids when low gas volume is involved in the source process. Therefore, we estimate the crack size for the case of basalt and water, respectively. Although an assumption about the crack geometry of the source may not seem completely justified, we believe that this is a realistic case because of the non-isotropic source

Please cite this article as: Lokmer, I., et al., Temporal evolution of long-period seismicity at Etna Volcano, Italy, and its relationships with the 2004–2005 eruption, Earth Planet. Sci. Lett. (2007), doi:10.1016/j.epsl.2007.11.017

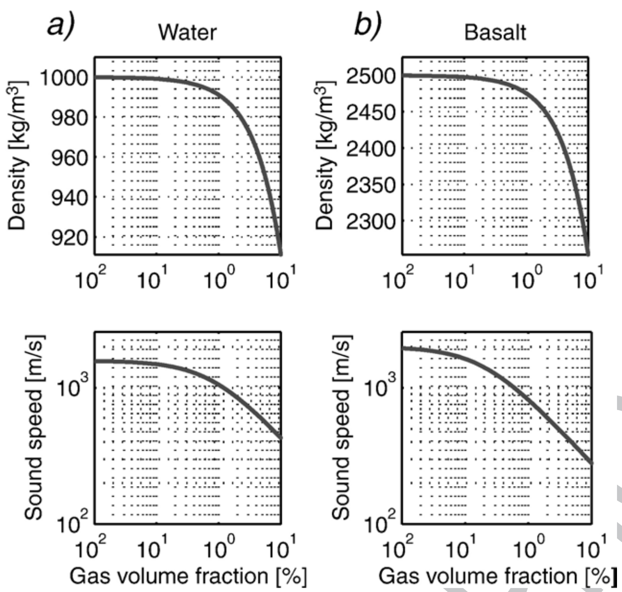

Fig. 8. Density and speed of sound in (a) water and (b) basalt for a 0.01 – 10% of the gas volume fraction in a fluid–gas mixture. The speed of sound was calculated using the model of Commander and Prosperetti (1989). The temperature of water was set to 120 °C and initial speed to 1580 m/s, while these values for basalt were 1100 °C and 2000 m/s, respectively.

radiation observed by Saccorotti et al. (2007), the change of polarisation of the mode of oscillation and geological setting of the source region. This is also the most natural geometry satisfying mass transport beneath a volcano (Kumagai et al., 2002).

Apart from the crack stiffness, values of the acoustic velocity and density of the fluid are needed for an estimation of the crack size. In our calculations, we allowed a gas volume fraction in fluid to lie within the range 0.01%–2%. We obtained velocities for bubbly basalt and water with a bubble radius of 1 mm from the model for bubbly liquids of Commander and Prosperetti (1989), using equations (75)–(86) in Chouet (1996a,b) and neglecting the surface tension of the bubbles. The initial values in the model, for pure basalt at a pressure of 20 MPa and a temperature of 1100 °C, were: velocity c=2000 m/s (Chouet [9]), and density ρ=2500 kg/m^3. At the same pressure and a temperature of 120 °C, for pure water we used c=1580 m/s (Benedetto et al., 2005) and ρ=1000 kg/m^3. Following Saccorotti et al. (2001), variation in the density of the fluid–gas mixture with the gas volume fraction was calculated using the following set of equations:

$$\rho = n\rho_g + (1-n)\rho_f$$
$$\rho_g = \frac{p}{RT}, \tag{7}$$

where ρ is the density of the mixture, n the gas volume fraction, ρ_g density of the gas, ρ_f the density of the pure fluid, p pressure, R the individual gas constant and T temperature. Both variations of velocity and density for basalt and water at poor gas volume fraction are given in Fig. 8. It can be seen that for a gas volume fraction in a range 0.01% – 2%, the acoustic velocity in basalt takes values between 1500 m/s and 600 m/s, in water between 1300 m/s and 800 m/s, while the drop of densities is much lower. Assigning a P-wave velocity in the host rock to 3000 m/s (Patane et al., 2001), the estimated impedance contrast between the host rock and basalt ranges between 1.6 and 5.4, thus overlapping with the 1.5–7.5 range for andesite, used by Neuberg et al. (2000) in their modelling of LP activity at Montserrat. Slightly higher impedance contrast for andesitic volcanoes could be explained by the lighter and gas-richer andesitic magmas. However, the estimated ranges of values overlap significantly, thus suggesting that similar parametrisation can be used for modelling of resonant sources on both types of volcanoes.

We estimate the velocity of the crack waves sustaining the source resonance from the theoretical dispersion curves. According to Ferrazzini and Aki (1987), who first analytically described the existence of the slow waves at the fluid–solid interface, the dispersion relation for the slow wave velocity, for a Poisson's ratio $\sigma = 0.25$, can be written as:

$$\coth\left[\sqrt{1-\left(\frac{v}{a}\right)^2}\cdot\left(\frac{\pi h}{\lambda}\right)\right] = -\frac{\rho_s}{\rho_f}\frac{\sqrt{1-\left(\frac{v}{a}\right)^2}}{\left(\frac{v}{\beta}\right)^4}\cdot\left[\frac{\left(2-\left(\frac{v}{\beta}\right)^2\right)^2}{\sqrt{1-\left(\frac{v}{a}\right)^2}} - 4\sqrt{1-\left(\frac{v}{\beta}\right)^2}\right] \tag{8}$$

where v is the slow wave velocity, a the acoustic velocity, h is the channel thickness, λ is wavelength, β is the S-wave velocity in the solid, and ρ_f and ρ_s are the densities of the fluid and solid, respectively. By taking $\beta = 1730$ m/s (e.g. Patanè et al., 2002), $\rho_s = 2650$ kg/m^3, and assuming the fundamental mode of the crack oscillation, $\lambda = L$, combining Eqs. (6) and (8) gives the dependence of the ratio v/a on the crack stiffness, C, as shown in Fig. 9. Note that dispersion curves depend only slightly on the velocities and densities of fluid within our range of interest (see also Chouet, 1996a,b, Fig. 14). Therefore, only the curves calculated for the average velocities and densities are given in the diagram. Ferrazzini and Aki (1987) showed that for the calculation of the fundamental mode of resonance ($\lambda = L$), one half of the value of the ratio v/a given by theoretical curve should be used. Thus, for the range of values of the crack stiffness marked in the diagram ($C = 100$–500 for basalt, and $C = 10^3$–$5\cdot 10^3$ for water), we estimated the ratio $v/a = 0.15$–0.07 for basalt and $v/a = 0.048$–0.024

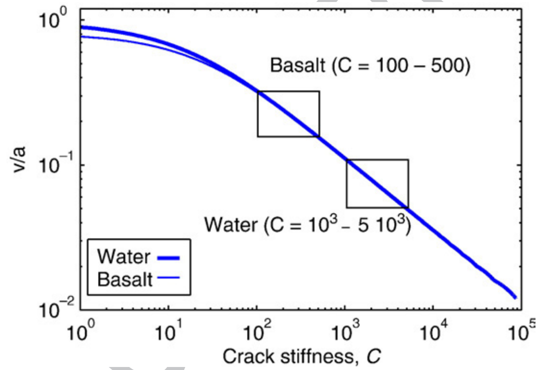

Fig. 9. Theoretical dependence of the slow wave velocity in a crack of infinite length on the crack stiffness defined as $C = (b/\mu)(\lambda/h)$, for water and basalt. For the crack of finite dimensions, the value v/c for the fundamental mode of resonance is about one half of the value obtained from the diagram. Realistic values of the crack stiffness for the crack filled by basalt and water, respectively, are shown in the figure.

for water. For the fundamental longitudinal mode, the crack length and its aperture can be estimated from the following relations:

$$L = \frac{v}{f} = \frac{v}{a}\cdot\frac{a}{f}, \tag{9}$$

where f is frequency, and

$$h = \frac{b}{\mu}\frac{L}{C}. \tag{10}$$

The same approach can be used for estimation of the crack width, by defining the transverse crack stiffness, C_t, as follows:

$$C_t = \frac{b}{\mu}\frac{W}{h}, \tag{11}$$

where W denotes the crack width, h its aperture, μ is rigidity and b is the bulk modulus of the fluid. For the case of basalt, our estimated crack length varies between 105 and 563 m, while its aperture takes values between 0.02 and 3.9 m. If the fluid is water, these values are $L = 48$–179 m and $h = 1$–38 mm. The ratio between the width and the length of the crack is about $W/L = 0.85$ for both cases.

We have used the mode with wavelength L to estimate the crack size. There is no clear justification for the choice of the mode L, except that it is the fundamental mode for a crack excitation triggered by a pressure step applied at its perimeter (Fig. 1 and Table 2 in Chouet, 1986), a scenario suggested by our proposed model. If we used instead the next higher mode, $2L/3$, which is at the same time the lowest dominant mode for a crack excitation triggered at the centre of the crack (Kumagai and Chouet, 2000; Kumagai et al., 2002), the estimated crack size would be about twice as big as for the mode L. Although based on a host of assumptions, the estimated dimensions seem quite realistic for both types of fluid involved in the source process. In theory, moment-tensor inversion may help us to distinguish between these two possibilities, based on the estimated expected amplitudes at seismic stations for the resolved source orientation and its volumetric change. However, as seen above, the estimated source size values overlap, thus producing an overlapping range of values for the displacement at the source for the two types of fluids. For instance, a volumetric change of 150 m^3, estimated by Saccorotti et al. (2007) for the VLP source, gives a displacement of the crack walls between 0.6 mm and 1.6 cm for basalt, i.e. between 6 mm and 8 cm for water. Neglecting the radiation pattern of the source and assuming geometrical spreading as a primary factor

Please cite this article as: Lokmer, I., et al., Temporal evolution of long-period seismicity at Etna Volcano, Italy, and its relationships with the 2004–2005 eruption, Earth Planet. Sci. Lett. (2007), doi:10.1016/j.epsl.2007.11.017

influencing the amplitude decay, then expected amplitude at ECPN station can be roughly estimated by:

$$A_{\mathrm{ECPN}} = A_0/r^b, \tag{12}$$

where A_{ECPN} denotes amplitude of displacement at ECPN station, A_0 is the amplitude at the source and r^b is the geometrical spreading factor with b taking values of 0.5, 1 or 2, for surface waves, far-field body waves and near-field term, respectively. Applying the Eq. (12) to the whole estimated range of values of displacement at the source (0.6 mm–8 cm), and putting $r=1.5$ km, the exponent b needs to take values between 0.6 and 1.2 in order to produce an average displacement of 10 μm recorded at ECPN station (Fig. 2). Since the wavefield is recorded in the near-field, where all types of waves are intertwined, it is impossible to a priori assign a value of b. Moreover, the situation is further complicated by a number of factors, such as the scattering of the wavefield on the pronounced topography, uncertainties in the shallow part of the velocity model responsible for amplification of the signal, the wide range of amplitudes recorded at the surface and the finite dimensions of the source. All these suggest that, without a detailed velocity model of the upper part of the volcano and extensive numerical simulations, seismological techniques alone are not enough to distinguish between the types of fluids involved in the LP source process at Etna. This work will be the subject of further investigations.

5. Concluding remarks

In this paper we have analysed the temporal evolution of LP–VLP activity which occurred at Etna Volcano from November 2003 to August 2005, thus encompassing the effusive eruption taking place between September 2004 and March 2005. We extended the work of Saccorotti et al. (2007) who analysed a pre-eruptive sequence of LP activity and proposed a model where the gas slug formed within the magmatic column being injected into an overlying cavity filled with either magmatic or hydrothermal fluids. Although they did not find a link between the observed LP activity and the eruption, this work suggests that such a link was established at the latter end of the eruptive sequence, most likely as a consequence of a reestablishment of the pressure balance in the plumbing system, after it was undermined due to discharge of large amounts of resident magma during the eruption. Such a scenario successfully explains the observed increase of the recorded displacement after the eruption as well as an increase of both frequency and Q factors of the source resonance. Furthermore, due to the non-isotropic source radiation observed by Saccorotti et al. (2007), a change of polarisation of the mode of oscillation and geological setting of the source region inferred from a number of geophysical studies, a crack represents the most like source geometry. This is also the most natural geometry satisfying mass transport beneath a volcano (Kumagai et al., 2002). In this context, the observed difference in the polarisation of signal before and after the eruption can be explained by the transition from longitudinal to transversal crack resonance due to the newly established equilibrium between the lithostatic pressure and the local stress field after the eruption. The estimated size of the basalt- and water-filled cracks, respectively, seems to be within a realistic range of values expected for Etna volcano.

We can summarize our interpretation as follows:

1) pressure drop due to the void left by the erupted material
2) this pressure drop leads to a deeper gas nucleation level (a larger gas slug arrives to the terminal part of the conduit (we see it as a deeper VLP source)
3) as a consequence of 2), more gas is injected into the crack (bigger events in Period II than in Period I (which we observe)
4) a new stress regime established by the eruption changes the direction in which the crack is discharging into the surrounding medium (changing the polarisation of the signal)

Despite both location results and waveform similarity indicating negligible source movement, the polarisation attributes change markedly. We attribute this change to a modification of the way in which the crack discharges fluid, as a consequence of a changing stress regime. This aspect suggests that, under particular conditions, LP could also act as possible stress gauges.

This study reveals a different concept for the generation of LP events, to one described in Falsaperla et al. (2002) where the LP activity is explained as a consequence of dyke pressurization due to the collapse of the crater floor. Also, our model is different from the Stromboli case, where, as opposed to the interaction between the two systems suggested here, VLP and LP oscillations originate in the same system, representing the volumetric deformation and LP oscillation of a shallow crack, respectively (Chouet et al., 2003). This indicates that a wide variety of phenomena can cause the same type of seismological observations and puts an imperative on the closer cooperation between different geophysical and geological disciplines involved in the

Please cite this article as: Lokmer, I., et al., Temporal evolution of long-period seismicity at Etna Volcano, Italy, and its relationships with the 2004–2005 eruption, Earth Planet. Sci. Lett. (2007), doi:10.1016/j.epsl.2007.11.017

widening our knowledge about the complex physical processes beneath volcanoes.

Acknowledgements

This work was part financed by the INGV-Department for Civil Protection and EU 6th framework project VOLUME. Ivan Lokmer is supported by the EU 6th framework Marie Curie RTN, SPICE. High-end computational resources needed for the 3D simulations were provided by the Irish national project COSMOGRID, funded by the Irish Higher Education Authority and Irish Centre for High End Computing (ICHEC). The paper has been improved through fruitful discussions with Flor de Lis Mancilla Pérez. Gareth O'Brien is acknowledged for his assistance in the computational aspects of this work.

References

Akaike, H., 1974. A new look at the statistical model identification. IEEE Trans. Automat. Contr. AC-19, 716–723.

Aki, K., Richards, P.G., 2002. Quantitative Seismology, second ed. University Science Books, Sausalito, California.

Aki, K., Fehler, M., Das, S., 1977. Source mechanism of volcanic tremor: Fluid-driven crack models and their application to the 1963 Kilaeua eruption. J. Volcanol. Geotherm. Res. 2, 259–287.

Behncke, B., Neri, M., 2003. The July–August 2001 eruption of Mt. Etna (Sicily). Bull. Volcanol. 65, 461–476.

Benedetto, G., Gavioso, R.M., Giuliano Albo, P.A., Lago, S., Madonna Ripa, D., Spagnolo, R., 2005. Speed of sound in pure water at temperatures between 274 and 394 K and pressures up to 90 MPa. Int. J. Thermophys 26. doi:10.1007/s10765-005-8587-2.

Bonacorso, A., Davis, P.M., 2004. Modelling of ground deformation associated with recent lateral eruptions: Mechanisms pf magma ascent and intermediate storage at Mt. Etna. In: Bonacorso, A., Calvari, S., Coltelli, M., Del Negro, C., Falsaperla, S. (Eds.), Mt. Etna: Volcano Laboratory. American Geophysical Union, Washington DC, pp. 293–306.

Burton, M.R., Neri, M., Andronico, D., Branca, S., Caltabiano, T., Calvari, S., Corsaro, R.A., Del Carlo, P., Lanzafame, G., Lodato, L., Miraglia, L., Salerno, G., Spampinato, L., 2005. Etna 2004–2005: an archetype for geodinamically-controlled effusive eruptions. Geophys. Res. Lett. 32, L09303. doi:10.1029/2005GL022527.

Chouet, B.A., 1986. Dynamics of a fluid-driven crack in three dimensions by the finite difference method. J. Geophys. Res. 91, 13967–13992.

Chouet, B.A., 1988. Resonance of a fluid-driven crack: Radiation properties and implications for the source of long-period events and harmonic tremor. J. Geophys. Res. 93, 4375–4400.

Chouet, B.A., 1992. A seismic model for the source of long-period events and harmonic tremor. In: Gasparini, P., Scarpa, R., Aki, K. (Eds.), Volcanic Seismology. Springer-Verlag, Berlin, pp. 133–156.

Chouet, B.A., 1996a. Long-period volcano seismicity: its source and use in eruption forecasting. Nature 380, 309–316.

Chouet, B.A., 1996b. New methods and future trends in seismological volcano monitoring. In: Scarpa, R., Tilling, R.I. (Eds.), Monitoring and Mitigation of Volcano Hazards. Springer, Berlin, pp. 80–82.

Chouet, B.A., 2003. Volcano seismology. PAGEOPH 160, 739–788.

Chouet, B., Julian, B.R., 1985. Dynamics of an expanding fluid-filled crack. J. Geophys. Res. 90, 11184–11198.

Chouet, B.A., Page, R.A., Stephens, C.D., Lahr, J.C., Power, J.A., 1994. Precursory swarms of long-period events at Redoubt Volcano (1989–1990), Alaska: their origin and use of a forecasting tool. J. Volcanol. Geotherm. Res. 62, 95–135.

Chouet, B.A., Saccorotti, G., Martini, M., Dawson, P.B., De Luca, G., Milana, G., Scarpa, R., 1997. Source and path effects in the wavefields of tremor and explosions at Stromboli volcano, Italy. J. Geophys. Res. 102, 15129–15150.

Chouet, B.A., Dawson, P., Ohminato, T., Martini, M., Saccorotti, G., Giudicepietro, F., De Luca, G., Milana, G., Scarpa, R., 2003. Source mechanisms of explosions at Strmboli Volcano, Italy, determined from moment-tensor inversions of very-long-period data. J. Geophys. Res. 108, 2019. doi:10.1029/2002JB001919.

Commander, K.W., Prosperetti, A., 1989. Linear pressure waves in bubbly liquids: comparison between theory and experiments. J. Acoust. Soc. Am. 85, 732–746.

Corsaro, R.A., Miraglia, L., 2005. Dynamics of 2004–2005 Mt. Etna effusive eruption as inferred from petrologic monitoring. Geophys. Res. Lett. 32, L13302. doi:10.1029/2005GL022347.

De Gori, P., Chiarabba, C., Patanè, D., 2005. Qp structure of Mount Etna: Constraints for the physics of the plumbing system. J. Geophys. Res. 110, B05303. doi:10.1029/2003JB002875.

De Vries, P.G., 1986. Sampling theory for forest inventory, first ed. Springer-Verlag, New York.

Della Monica, G., Di Mario, R., Scandone, R., Cecere, G., Del Negro, C., De Martino, P., Santochirico, F., 2004. Electrical modelling of the shallow structural setting of the Cistemazza–Montanogla area (Mt. Etna). Quad. Geofis. 35, 39–44.

Di Grazia, G., Falsaperla, S., Langer, H., 2006. Volcanic tremor location during the 2004 Mount Etna lava effusion. Geophys. Res. Lett. 33, L04304. doi:10.1029/2005GL025177.

Falsaperla, S., Privitera, E., Chouet, B.A., Dawson, P.B., 2002. Analysis of long-period events recorded at Mt. Etna (Italy) in 1992 and their relationship to eruptive activity. J. Volcanol. Geotherm. Res. 114, 419–440.

Ferrazzini, V., Aki, K., 1987. Slow waves trapped in a fluid-filled infinite crack: Implication for volcanic tremor. J. Geophys. Res. 92, 9215–9223.

Kanasewich, E.R., 1981. Time sequence analysis in geophysics. University of Alberta Press, Edmonton, Alberta.

Kumagai, H., 2006. Temporal evolution of a magmatic dike system inferred from the complex frequencies of very long period seismic signals. J. Geophys. Res. 111, B06201. doi:10.1029/2005JB003881.

Kumagai, H., Chouet, B.A., 2000. Acoustic properties of a crack containing magmatic or hydrothermal fluids. J. Geophys. Res. 105, 25493–25512.

Kumagai, H., Chouet, B.A., Nakano, M., 2002. Temporal evolution of a hydrothermal system in Kasatsu–Shirane volcano, Japan, inferred from the complex frequencies of long-period events. J. Geophys. Res. 107, 2236. doi:10.1029/2001JB000653.

Kumazawa, M., Imanishi, Y., Fukao, Y., Furumoto, M., Yamamoto, A., 1990. A theory of spectral analysis based on the characteristic property of a linear dynamic system. Geophys. J. Int. 101, 613–630.

Manzella, A., Zaja, A., 2006. Volcanic structure of the southern sector of Mt. Etna after 2001 and 2002 eruptions defined by magnetotelluric measurements. Bull. Volcanol. 69, 41–50.

Martínez-Arévalo, C., Patanè, D., Rietbrock, A., Ibánez, J.M., 2005. The intrusive process leading to the Mt. Etna 2001 flank eruption:

Constraints from 3-D attenuation tomography. Geophys. Res. Lett. 32, L21309. doi:10.1029/2005GL023736.

Matsubara, W., Yomogida, M., 2004. Source process of low-frequency earthquakes associated with the 2000 eruption of Mt. Usu. J. Volcanol. Geotherm. Res. 134, 223–240.

Mauriello, P., Patella, D., Petrillo, Z., Siniscalchi, A., Iuliano, T., Del Negro, C., 2004. A geophysical study of the Mount Etna volcanic area. In: Bonacorso, A., Calvari, S., Coltelli, M., Del Negro, C., Falsaperla, S. (Eds.), Mt. Etna: Volcano Laboratory. American Geophysical Union, Washington DC, pp. 273–291.

Neuberg, J., Luckett, R., Ripepe, M., Braun, T., 1994. Highlights from a seismic broadband array on Stromboli volcano. Geophys. Res. Lett. 21, 749–752.

Neuberg, J., Baptie, B., Luckett, R., Stewart, R., 1998. Results from the broad-band seismic network on Montserat. Geophys. Res. Lett. 25, 3661–3664.

Neuberg, J., Luckett, R., Baptie, B., Olsen, K., 2000. Models of tremor and low-frequency earthquake swarms on Montserrat. J. Volcanol. Geotherm. Res. 101, 83–104.

O'Brien, G.S., Bean, C.J., 2004. A 3D discrete numerical elastic lattice method for seismic wave propagation in heterogeneous media with topography. Geophys. Res. Lett. 31, L14608. doi:10.1029/2004GL020069.

Ohminato, T., Chouet, B.A., Dawson, P., Kedar, S., 1998. Waveform inversion of very long period impulsive signals associated with magmatic injection beneath Kilauea Volcano, Hawaii. J. Geophys. Res. 103, 23839–23862.

Patanè, D., Chiarabba, C., Cocina, O., De Gori, P., Moretti, M., Boschi, E., 2002. Tomographic images and 3D earthquake locations of the seismic swarm preceding the 2001 Mt. Etna eruption: Evidence for a dyke intrusion. Geophys. Res. Lett. 29, 135–138.

Ripperger, J., Igel, H., Wasserman, J., 2003. Seismic wave simulation in the presence of real volcano topography. J. Volcanol. Geotherm. Res. 128, 31–44.

Saccorotti, G., Chouet, B., Dawson, P., 2001. Wavefield properties of a shallow long-period event and tremor at Kilaeua Volcano, Hawaii. J. Volcanol. Geotherm. Res. 109, 163–189.

Saccorotti, G., Lokmer, I., Bean, C.J., Di Grazia, G., Patanè, D., 2007. Analysis of sustained long-period activity at Etna Volcano, Italy. J. Volcanol. Geotherm. Res. 160, 340–354.

Sturton, S., Neuberg, J., 2003. The effects of a decompression on seismic parameter profiles in a gas-charged magma. J. Volcanol. Getherm. Res. 128, 187–199.

Tarantola, A., Vallette, B., 1982. Inverse problem = quest for information. J. Geophys. 50, 159–170.

Please cite this article as: Lokmer, I., et al., Temporal evolution of long-period seismicity at Etna Volcano, Italy, and its relationships with the 2004–2005 eruption, Earth Planet. Sci. Lett. (2007), doi:10.1016/j.epsl.2007.11.017